ISSN: 2633-4828 Vol. 5 No.4, December, 2023

International Journal of Applied Engineering & Technology

A STUDY ON THE MICROSTRUCTURAL AND MECHANICAL PROPERTIES OF IN718 PROCESSED THROUGH LASER DIRECT ENERGY DEPOSITION AND CONVENTIONAL CASTING

Bhushandada Sandipan Navgire[1*], Vivek Kumar Singh[2], Sushil Mishra[3] and Divya Padmanabhan[4]
[1,4]Department of Mechanical Engineering, Pillai College of Engineering Panvel, Navi Mumbai - 410206, India
[2,3]Department of Mechanical Engineering, Indian Institute of Technology Bombay, Mumbai – 400076, India
[1]bhushandada05@gmail.com, [2]viveksmech11@gmail.com, [3]sushil.mishra@iitb.ac.in and [4]divyamvp@mes.ac.in
ORCID iD: 0009-0000-6319-0735

ABSTRACT
Inconel 718 is employed in high temperature applications because of its high temperature mechanical qualities and excellent weldability. Nearly half of the parts used in jet engines are made of nickel superalloy. This study compares the Inconel 718's (IN718) mechanical and microstructural properties that is additively produced (AM) against IN718 that is cast conventionally. Few studies have been conducted on the AM process of laser direct energy deposition (L-DED) using wire as a feedstock material to create IN718 samples. Three interlayer rotation angles: 0º, 67º and 90º are used to produce IN718 coupons. Columnar dendritic structure along with secondary phase such as Laves phase are present in L-DED parts. Laves phase are the intermetallic structure formed during micro-segregation of solute during solidification. The mechanical test revel an excellent strength and ductility of L-DED parts as compared to the as-cast parts. Among the three inter-layer strategy used for L-DED processing, 0º samples showed the best ductility. The structure and characteristics of L-DED parts, as well as a comparison with traditionally made parts, are clarified by this work.

Keywords: Additive Manufacturing, Direct Energy Deposition, IN718, Laves phase, EBSD

1. INTRODUCTION
Additive production (AM), which deviates significantly from traditional production techniques, is a cutting-edge strategy that is precisely outlined in the strict ASTM F2792-12a standard. This creative method involves the skilful combination of various materials to create real items. It carefully uses 3D model data, frequently working layer by layer. Emphasizing that the additive manufacturing (AM) business is presently undergoing a remarkable upsurge marked by exponential expansion in our modern day is crucial [1]. This rapid expansion across numerous industries demonstrates the adaptability and potential of AM. Its uses have expanded to include anything from the large-scale production of vital components for the aerospace industry to the custom fabrication of complex medical equipment, making it an increasingly alluring option for a variety of sectors [2]. When AM is compared to traditional production, a distinct set of benefits and drawbacks become apparent. This is where additive manufacturing (AM) excels because of its innate ability to create complex, customized shapes, produce parts that get close to the desired "near net shape," and—perhaps most exciting of all—provide mechanical qualities that are on par with or even better than those of subtractive manufacturing techniques [2-4]. This technological marvel's foundational process uses metal wires as its main feedstock, and the AM process known as laser wire Direct Energy Deposition (L-DED) puts laser energy front and centre. The application of superalloys based on nickel in AM is particularly interesting. Interestingly, around half of the parts used in jet engines are made of nickel superalloys, which are highly valued for their exceptional strength at high temperatures and creep resistance. For this reason, the quest for nickel superalloy processing via AM channels is highly intriguing [5]. The Inconel 718 alloy stands out as a superior option among the wide range of nickel-based superalloys. The oil and aerospace industries both use it extensively [6,7], and it has an advantage over other nickel superalloys in terms of weldability, which heightens its allure [8]. Particularly, the laser-based Additive Manufacturing (AM) solidification process is known to produce a significant amount of what is referred to as the "Laves phase," which is essential for the separation of alloying elements from the liquid phase, including Molybdenum (Mo) and Niobium (Nb) [9–12]. The primary rationale for Nb elements' absence from the γ phase is their restricted

solubility in it. The beginning of solidification is caused by the phase change from the liquid to the γ phase, which is an important point in the process. There is a significant increase in the Nb content in the liquid phase during this phase transition. This increase in Nb atoms in the liquid phase is directly related to a significant amount of Nb atoms being ejected from the γ phase and finding new homes in the liquid phase via the complex dendritic liquid interface, which occurs after γ dendrites form [13, 14]. The liquid phase's chemical composition changes while solidification advances unabatedly, gradually moving in the direction of the eutectic point. The result of this transition is the creation of a coexisting state in which the γ phase and the liquid phase coexist peacefully. It is impossible to overstate the importance of the Laves phase because studies have conclusively demonstrated that protracted Laves phases in the interdendritic areas are detrimental to a number of important factors. It has a negative effect on a material's mechanical properties [15, 16], its resilience to high-cycle fatigue [12, 17, 18], and its susceptibility to corrosion. Because of this, engineers and scientists have worked hard to investigate a variety of approaches to address the problem that the development of Laves phases presents. These tactics cover a variety of cutting-edge methods, such as employing pulsed laser techniques rather than continuous beams, switching to flat-headed laser profiles from Gaussian ones, and even purposefully lowering the alloy's Nb concentration. However, it's important to note that heat treatment has become the most popular and extensively used post-processing technique to efficiently break down the Laves phase and encourage the formation of phases that are suitable for precipitation-hardening [11,20–24]. Using AM to its maximum potential in the context of modern materials engineering has shown to be made possible in large part by this strategy. Many creative approaches have been carefully investigated to address the daunting problem of the Laves phase's creation. These diverse strategies include cutting-edge methods, like replacing a continuous laser beam with a pulsed laser source [12, 19]. Furthermore, instead of using the traditional Gaussian laser profile, researchers have investigated using a flat-headed laser profile, which provides a new perspective on how to handle Laves phase issues [10]. Further research has involved purposefully lowering the Niobium (Nb) concentration in the alloy matrix, which adds to a more sophisticated strategy to lessen the formation of the Laves phase [18]. But it is crucial to emphasize that heat treatment has been the most popular and effective post-processing technique for effectively breaking down the Laves phase and promoting the formation of the desired precipitation-hardenable phases [11,20–24]. Because of its effectiveness in realizing Additive Manufacturing's (AM) full potential within the framework of modern materials engineering, this technique has gained popularity. It is important to note that there hasn't been much research done on the AM method using wire as a feedstock material for laser Direct Energy Deposition (L-DED) in order to create IN718 samples. This work aims to conduct a thorough comparison between the mechanical and microstructural properties of Inconel 718 (IN718) fabricated using additive manufacturing (AM) and IN718 cast conventionally. In this study, wire is used as a feedstock material, and the AM technique of laser direct energy deposition (L-DED) is specifically examined. Three different interlayer rotation angles (0º, 67º, and 90º) are skilfully used for the creation of IN718 coupons in order to identify and clarify any subtle differences in the material's characteristics and functionality.

2. MATERIALS AND METHODS

Material Processing. For this work, the preferred device for additive manufacturing of Inconel 718 samples was the sophisticated Meltio M450 metal printer, which used the cutting-edge Laser-Direct Energy Deposition (L-DED) technology. With a powerful 1.2 kW diode laser that emits light at 976 nm, the Meltio M450 has a large print envelope that measures 145 mm by 168 mm by 390 mm. The laser head is placed to strategically emit six beams of uniform power at equal distances along the outer perimeter, while the feedstock wire is introduced into the system in the center. This sophisticated printer is designed to provide accuracy and productivity in the additive manufacturing process. Carefully selected Inconel 718 wire with a diameter of 1 mm was used as the feedstock material to create these Inconel 718 samples. Table 1 provides important information on the chemical composition of this Inconel 718 wire, including its elemental makeup. Furthermore, Table 2 provides a thorough summary of the particular L-DED processing parameters, highlighting the crucial characteristics and circumstances applied during the manufacturing process. Three different inter-layer rotation angles (0º, 67º, and 90º) were carefully incorporated into a bi-linear scanning method that was carefully chosen in order to further the

additive manufacturing quest. In the pursuit of optimal material characteristics and structural integrity, these rotation angles signify a purposeful modification in the orientation of subsequent layers. It is important to remember that the as-cast samples that served as the foundation for the comparison were obtained from industrial channels using the suction casting method. SolidWorks software was used to carefully create the digital blueprint for the printing process, and Simplify3D was used to efficiently handle the complex slicing and subsequent development of G-code, which controls the printer's movements. The L-DED setup and printed components are shown visually in Fig. 1, which also gives a concrete example of the advanced technology used in this additive manufacturing study. This whole system, which is outfitted with cutting-edge hardware and software, is essential to expanding the knowledge and use of Inconel 718 in the context of additive manufacturing.

Table 1: It shows the chemical makeup of Inconel 718 wire.

Element	Ni	Fe	Cr	Ni + Ta	Mo	Ti	Al	C	Si + Mn
Wt. %	Bal.	20	19	5.2	3	0.9	0.5	0.05	0.4

Table 2: Process parameter for L-DED of IN718

Parameter	**Value**
Laser Power	1100 W
Scanning Speed	7.5 mm/s
Wire Feed Rate	9.6mm mm/s
Gas Flow Rate (Argon)	10 l/min
Energy Density	147 J/mm^3

Material Characterization

The specimens were carefully sliced using Wire-Electric Discharge Machining (W-EDM) to begin the process of preparing samples for microstructural and mechanical investigation. Then, a series of steps were taken with these painstakingly produced samples in order to systematically reveal their microstructural characteristics. To get a more refined surface, the initial step of this technique was mechanical polishing. Emery paper was used to start, and the grit size was gradually increased from 320 to 2500. This was followed by a second polishing stage using colloidal silica (MetSil40) with particles as small as 0.04 µm. Chennai METCO produced an advanced polishing setup that was the equipment used for this purpose. Etching the polished samples was the next important step. The samples were carefully treated with Kalling's reagent for 20 seconds, an essential step that helped to highlight and highlight the microstructural properties of the material. The method of choice for preparing the samples for Electron Backscattered Diffraction (EBSD) was electropolishing. During the electropolishing process, a 70% methanol, 20% perchloric acid, and 10% butanol solution was applied. This solution produced a flawless surface quality that was ideal for EBSD analysis when it was applied for 20 seconds at a voltage of 20 V. After that, the samples' microstructural characteristics and compositional mapping were documented and examined using an Energy Dispersive X-ray Spectroscopy (EDS) instrument that was attached to a Zeiss Gemini SEM 300 high-resolution scanning electron microscope. This sophisticated configuration allowed for a thorough analysis of the microstructure and element distribution in the samples. A Crossbeam SEM was interfaced with a Velocity EBSD detector in the field of Electron Backscattered Diffraction (EBSD), integrating state-of-the-art technology for an in-depth analysis. A granular picture of the microstructure was ensured by acquiring EBSD data at a magnification of 100X and a step size of 1 µm. With the careful use of TSL-OIM software, the EBSD data were post-processed and analyzed, providing important information about the crystallography and microstructural properties of the materials being studied. By using a complete analytical technique, it is possible to obtain profound insights into the mechanical and microstructural features of the samples and ensure that they are thoroughly characterized.

Tensile test samples with gauge lengths of 25 mm and thicknesses of 3 mm were cut using wire EDM in accordance with ASTM E8 subsize standard. The tensile coupon's schematic is shown in Fig. 2. At a strain rate of 10-3 s-1, the tensile test was conducted using the MTS tensile test system. During the tensile test, the strain was

monitored using a 25 mm extensometer. Using a Gemini300 Zeiss SEM, the tensile sample's fractography was completed.

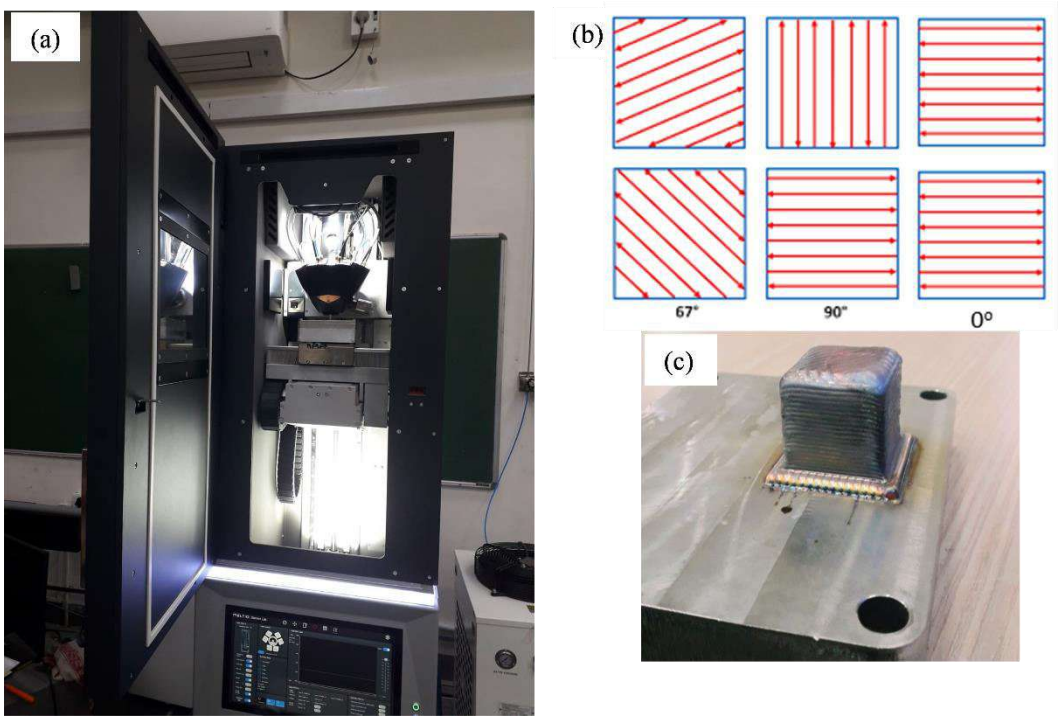

Fig. 1: (a) Meltio 450 setup, (b) three inter-rotations of 0º, 67º & 90º, and (c) printed Inconel 718 cube on SS316 base plate.

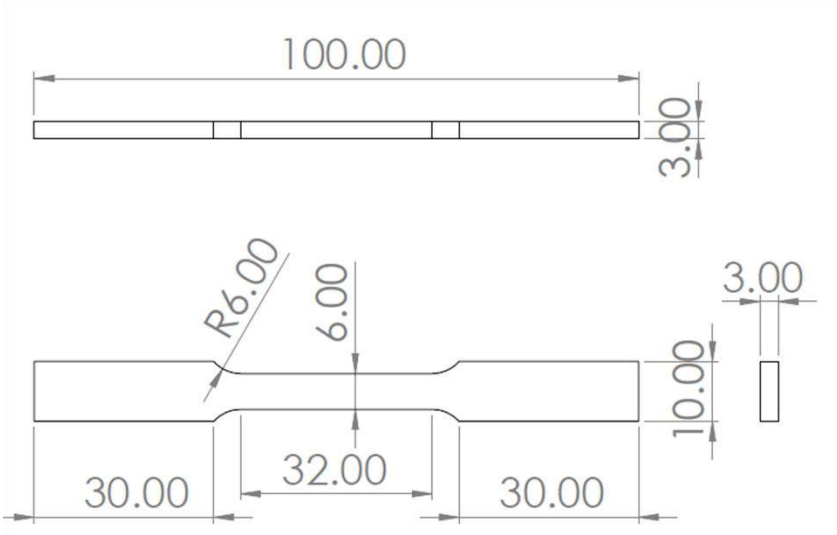

Fig. 2: Schematic with dimension of tensile coupon as per ASTM E8 standard.

3. RESULTS AND DISCUSSIONS:

Microstructure. The optical microstructure of the L-DED pieces in the construction direction is displayed in Fig. 3. The term "melt pool" refers to the continuous distribution of hemispherical shape that was produced during the direct energy deposition process. The width and depth of the melt pool are 3 mm and 1.25 mm, respectively. The SEM microstructure of the as-cast and L-DED samples is displayed in Fig. 4. The microstructure of the L-DED

sample in the build direction (BD) is shown in Fig. 4(a). Here, the secondary phase is shown by the light contrast, while the matrix phase is shown by the dark contrast. Solute atoms like Nb, Mo, and Ti microsegregate from the solidifying dendrite to the inter-dendritic liquid zone during the solidification of the melt pool in L-DED. Towards the end of solidification at the eutectic, a secondary phase forms as a result of the buildup of solute atoms Nb, Mo, and Ti at the interdendritic region. The Laves phase, an intermetallic phase of the topologically close-packed type consisting of (Ni, Fe, Cr)2(Nb, Mo, Ti) structure, is the secondary phase. Metal carbides are formed when elements such as Nb and Mo interact with carbon atoms that are rejected during solidification. The Laves phase formed at the eutectic as a result of additional rejection of this heavier element after the carbon atom was depleted. Laves phase is formed by the following solidification process: $L \rightarrow L+\gamma \rightarrow (L+NbC/\gamma) \rightarrow L+Laves/\gamma$ [12]. Fig. 4 (b) shows the microstructure of the L-DED part in plane oriented perpendicular to build direction and parallel to base plate. These equiaxed microstructure shows the cross-section of dendrite when viewed from the top plane. Here also segregates of solute atom are decorated at the inter-dendritic site. Fig. 4 (c) shows the as-cast microstructure to compliment the L-DED microstructure. A highly coarse microstructure is displayed by the as-cast part due to their lower solidification rate as compared to L-DED. As dendrites grow, the solidified dendrite's surface continually expels Nb from the solidifying γ - phase to the inter-dendritic liquid channel, driven by the differing solute solubilities in the two phases. This continuous rejection of Nb leads to an augmentation of Nb concentration within the liquid. Laves phase particles are found to be consistently present within these isolated regions enriched with Nb, separated by the dendritic arms, as the solidification process approaches its end and the dendritic arms coalesce and separate the liquid into distinct pockets. Therefore, the Laves phase onset is closely related to the extent of Nb segregation in these particular Nb-enriched areas.

The EDS results of the L-DED pieces orientated in the top plane and construction direction are shown in Fig. 5. The designated rectangular region is used to take the EDS maps. It indicates that there is a lot of Nb and Mo in the interdendritic region, which is indicative of the formation of the Laves phase. It is possible that the spherical phases, which are rich in Ti, are metal carbides in the form of TiC. Fig. 6 displays the inverse pole figure (IPF) for the L-DED and as-cast sample. In Fig. 6 (a), SD, TD and BD represents the scanning direction, transverse direction and build direction. Columnar microstructure is seen in the build direction while in the SD-TD plane an equiaxed kind of microstructure is displayed. A favored texture in <001> direction is shown which the direction of least resistance for the face centered cubic (FCC) crystals. The IPF map for the conventionally cast IN718 in Fig. 6 (b) shows the coarser equiaxed structure.

Fig. 3: Optical micrograph of 0º scanning strategy L-DED parts.

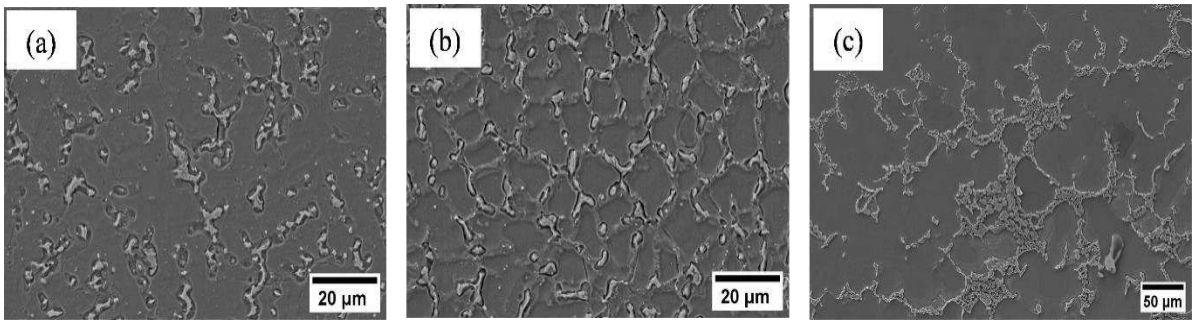

Fig. 4: SEM micrographs (a) for L-DED sample (0º inter-layer rotation) in build direction (b) L-DED sample taken at top surface parallel to base plate.

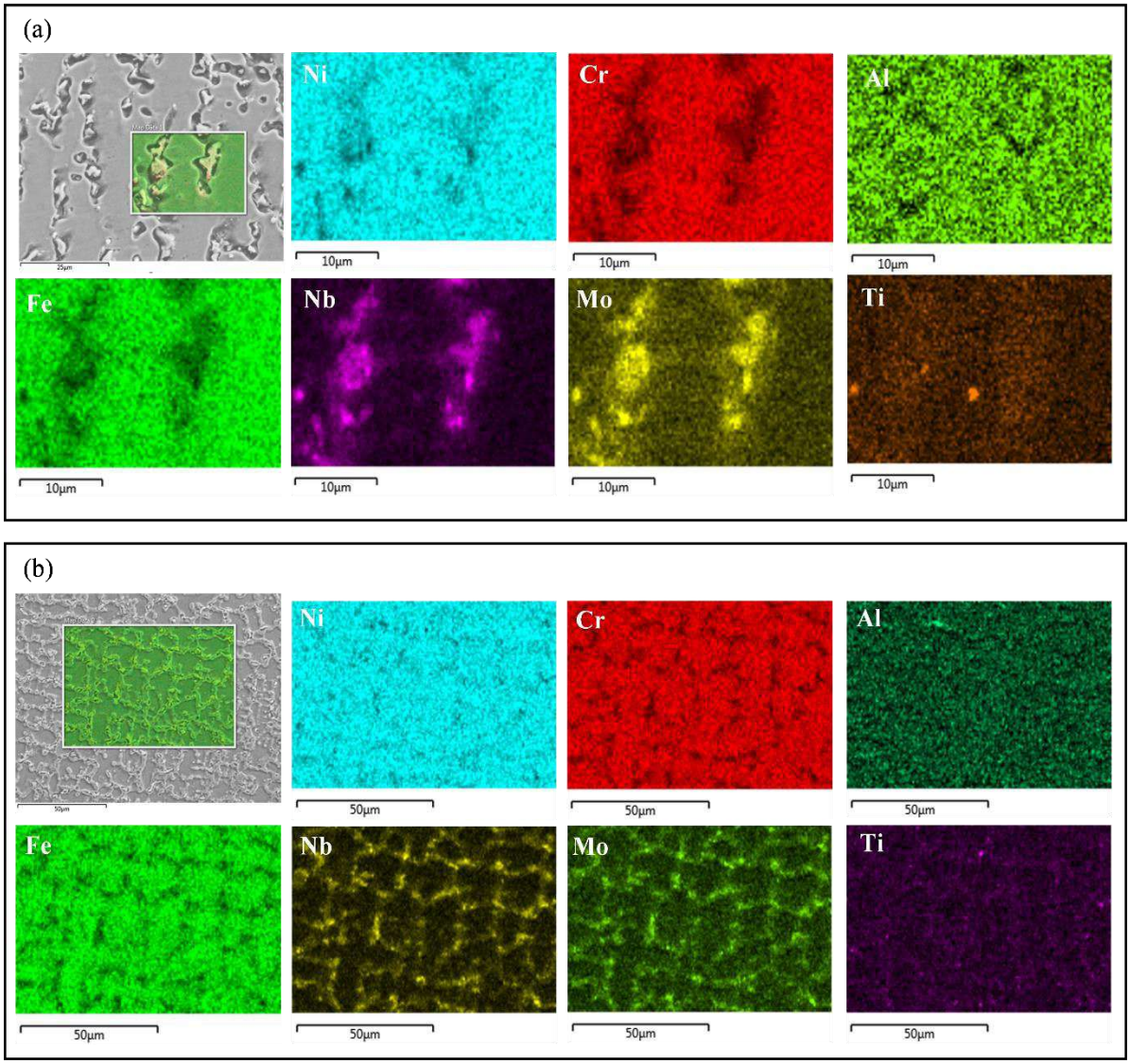

Fig. 5: EDS map of L-DED samples – (a) In the build direction and (b) top plane i.e., parallel to base plate.

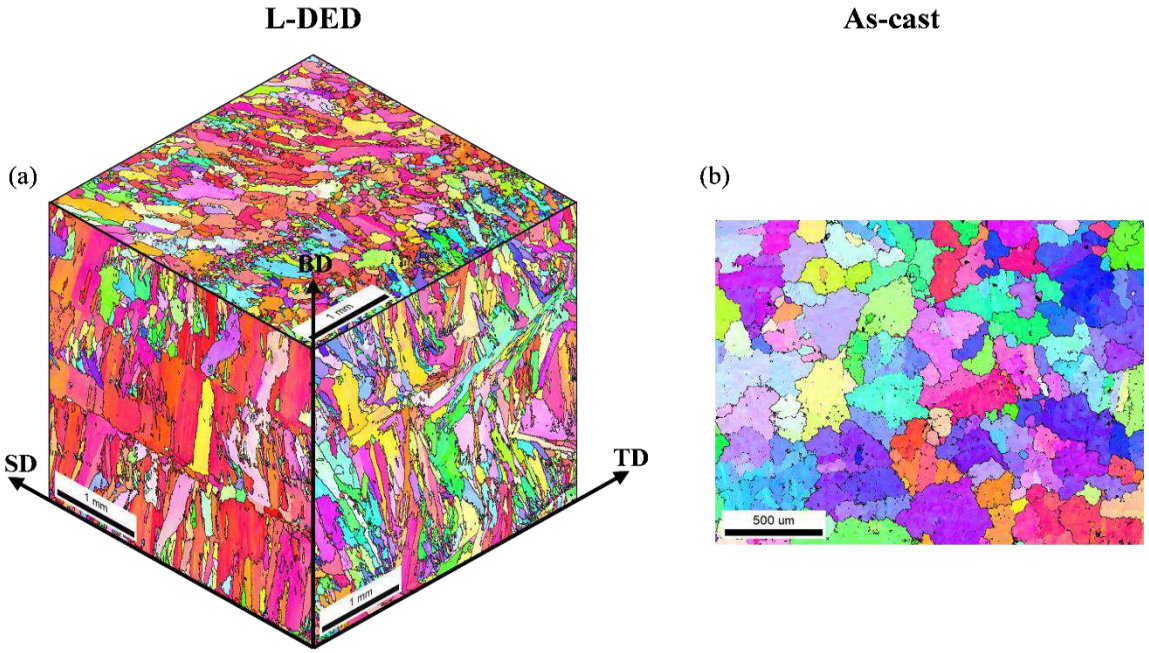

Fig. 6: Inverse pole figure (IPF) – (a) For L-DED sample in BD, SD and TD and (b) For as-cast sample.

Mechanical Performance. Tensile characteristics of Inconel 718 produced via traditional casting and the Laser Direct Energy Deposition (L-DED) process were investigated. The engineering stress-strain plot for the L-DED and as-cast samples, obtained from the tensile test, is shown in Fig. 7. Comparing L-DED samples to as-cast samples, the former demonstrated superior performance on the fronts of strength and ductility. The as-cast sample displayed a very poor ductility of only 4.5% as compared additively manufactured parts and their ultimate tensile strength is only (589 MPa). The L-DED part showed an almost similar tensile properties with an average UTS of 825 MPa and an average ductility of 34%. Among the L-DED samples the 0˚ scanning strategy condition showed a considerable better strength and ductility. On the other hand, it was determined that scan rotation angles had no discernible impact on the tensile characteristics of L-DED samples. The tensile properties for the L-DED and as-cast conditions are shown in Table 3.

The microstructure of the L-DED and conventional cast samples is the reason for the differences in their tensile strength values. The following illustrates how the principal dendritic arm spacing (PDAS) for Inconel 718 was formulated by Raghavan et al. [25]:

$$Kurz - Fisher\ Model: \lambda(\mu m) = 3195.214 \times G^{-0.5} \times R^{-0.25} \quad (1)$$

$$Trivedi\ Model: \lambda(\mu m) = 2145.952 \times G^{-0.5} \times R^{-0.25} \quad (2)$$

The L-DED condition has two order more thermal gradient than the casting process, which will lead finer structure in L-DED. Also, based on the microstructural results the PDAS for L-DED is 10 – 20 µm and for the cast samples PDAS is 100 – 200 µm. Therefore, due to the finer microstructure in L-DED, there is a higher strength as compared to conventional cast samples. By Hall -Petch relation $\sigma_y = \sigma_d + {k_y}/{\sqrt{d}}$, which provides the direction relation between grain size and yield strength explaining the higher yield strength in L-DED.

Fig. 8 provides the fractography of the L-DED tensile samples. It shows the presence of dimples signifying a ductile failure of parts. Fractography is the study and analysis of material fractures that involves looking at fractured surfaces to identify the causes and mechanisms of failure. It offers important details on fracture features such as fracture mode (ductile, brittle, etc.), crack propagation, morphology, and microstructural changes. Fractography enables the detection and characterization of characteristics like dimples, striations, cleavage facets, and fatigue-related features by utilizing methods like optical microscopy and scanning electron microscopy. Engineers can enhance materials, designs, and failure prevention techniques by using this research to help identify the kind and cause of fracture in areas including materials science, engineering, and failure analysis.

Table 3: Tensile properties (YS, UTS and elongation)

Conditions	Yield Strength (MPa)	UTS (MPa)	Elongation (%)
L-DED 0˚	554	862	39.26
L-DED 67˚	516	812	34.47
L-DED 90˚	521	851	30.61
As-cast	380	589	4.51

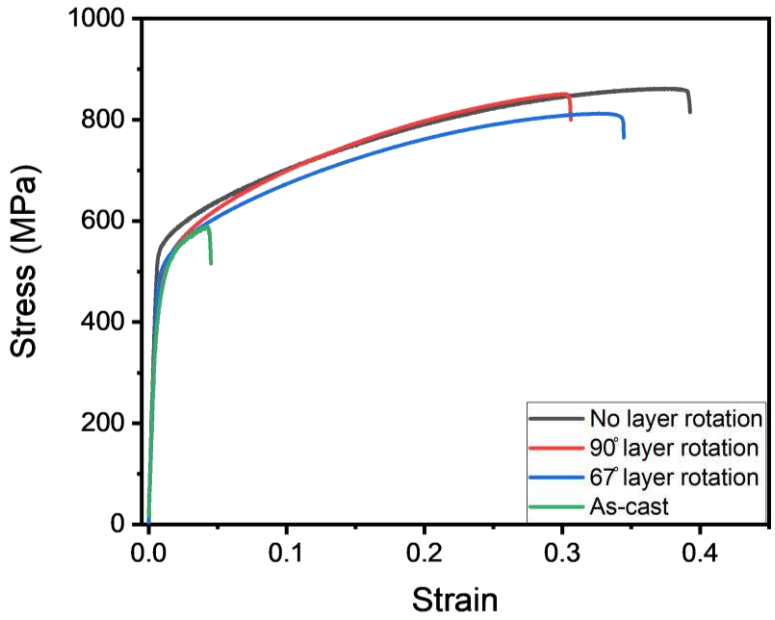

Fig. 7. Stress-strain plot obtain from tensile test for the L-DED samples with different inter-layer rotation and for the as-cast samples.

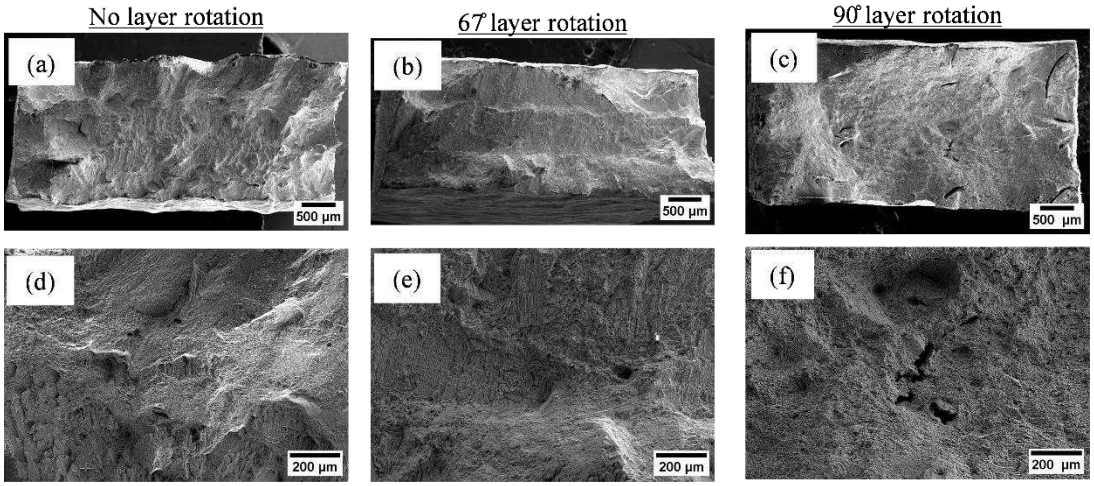

Fig. 8: Fracture surface of the tensile specimen for the L-DED samples – (a) for 0º inter-layer rotation, (b) for 67º inter-layer rotation, (c) for 90º inter-layer rotation and (d), (e) & (f) are the magnification image of (a), (b) & (c) respectively.

4. CONCLUSIONS

The additive manufacturing process qualifies to print components quickly and easily with complicated geometry and high quality. In this works a comparison of the structure and tensile properties between additively manufactured (AM) Inconel 718 (IN718) and conventionally cast IN718 sample was carried out. Primary columnar dendrites and secondary phase such as Laves phase are present in L-DED parts. Laves phase are the intermetallic structure formed during micro-segregation of solute atoms during solidification. The mechanical test revel an excellent strength and ductility of L-DED parts as compared to the as-cast parts. Among the three inter-layer strategy used for L-DED processing, 0º samples showed the best ductility.

REFERENCES

[1] S.A.M. Tofail, E.P. Koumoulos, A. Bandyopadhyay, S. Bose, L. O'Donoghue, C. Charitidis, Additive manufacturing: scientific and technological challenges, market uptake and opportunities, Mater. Today. 21 (2018) 22–37. https://doi.org/10.1016/j.mattod.2017.07.001.

[2] T. DebRoy, H.L. Wei, J.S. Zuback, T. Mukherjee, J.W. Elmer, J.O. Milewski, A.M. Beese, A. Wilson-Heid, A. De, W. Zhang, Additive manufacturing of metallic components – Process, structure and properties, Prog. Mater. Sci. 92 (2018) 112–224. https://doi.org/10.1016/j.pmatsci.2017.10.001.

[3] K. Kempen, L. Thijs, J. Van Humbeeck, J.P. Kruth, Mechanical Properties of AlSi10Mg Produced by Selective Laser Melting, Phys. Procedia. 39 (2012) 439–446. https://doi.org/10.1016/j.phpro.2012.10.059.

[4] L.C. Zhang, H. Attar, M. Calin, J. Eckert, Review on manufacture by selective laser melting and properties of titanium based materials for biomedical applications, Mater. Technol. 31 (2016) 66–76. https://doi.org/10.1179/1753555715Y.0000000076.

[5] T. Okura, Materials for Aircraft Engines, Aircr. Propuls. Final Rep. ASEN 5063 (2015) 1–14.

[6] D.F. Paulonis, J.J. Schirra, Alloy 718 at Pratt & Whitney - Historical perspective and future challenges, Proc. Int. Symp. Superalloys Var. Deriv. 1 (2001) 13–23. https://doi.org/10.7449/2001/superalloys_2001_13_23.

[7] K.N. Amato, S.M. Gaytan, L.E. Murr, E. Martinez, P.W. Shindo, J. Hernandez, S. Collins, F. Medina, Microstructures and mechanical behavior of Inconel 718 fabricated by selective laser melting, Acta Mater. 60 (2012) 2229–2239. https://doi.org/10.1016/j.actamat.2011.12.032.

[8] S. Catchpole-Smith, N. Aboulkhair, L. Parry, C. Tuck, I.A. Ashcroft, A. Clare, Fractal scan strategies for selective laser melting of 'unweldable' nickel superalloys, Addit. Manuf. 15 (2017) 113–122. https://doi.org/10.1016/j.addma.2017.02.002.

[9] S. Sui, J. Chen, Z. Li, H. Li, X. Zhao, H. Tan, Investigation of dissolution behavior of laves phase in inconel 718 fabricated by laser directed energy deposition, Addit. Manuf. 32 (2020) 101055. https://doi.org/10.1016/j.addma.2020.101055.

[10] Y. Chen, Y. Guo, M. Xu, C. Ma, Q. Zhang, L. Wang, J. Yao, Z. Li, Study on the element segregation and Laves phase formation in the laser metal deposited IN718 superalloy by flat top laser and gaussian distribution laser, Mater. Sci. Eng. A. 754 (2019) 339–347. https://doi.org/10.1016/j.msea.2019.03.096.

[11] S. Sui, H. Tan, J. Chen, C. Zhong, Z. Li, W. Fan, A. Gasser, W. Huang, The influence of Laves phases on the room temperature tensile properties of Inconel 718 fabricated by powder feeding laser additive manufacturing, Acta Mater. 164 (2019) 413–427. https://doi.org/10.1016/j.actamat.2018.10.032.

[12] H. Xiao, S. Li, X. Han, J. Mazumder, L. Song, Laves phase control of Inconel 718 alloy using quasi-continuous-wave laser additive manufacturing, Mater. Des. 122 (2017) 330–339. https://doi.org/10.1016/j.matdes.2017.03.004.

[13] C. Kumara, A.R. Balachandramurthi, S. Goel, F. Hanning, J. Moverare, Toward a better understanding of phase transformations in additive manufacturing of Alloy 718, Materialia. 13 (2020) 100862. https://doi.org/10.1016/j.mtla.2020.100862.

[14] O. Gokcekaya, T. Ishimoto, S. Hibino, J. Yasutomi, T. Narushima, T. Nakano, Unique crystallographic texture formation in Inconel 718 by laser powder bed fusion and its effect on mechanical anisotropy, Acta Mater. 212 (2021). https://doi.org/10.1016/j.actamat.2021.116876.

[15] G.D.J. Ram, A.V. Reddy, K.P. Rao, G. Madhusudhan, G.D.J. Ram, A.V. Reddy, K.P. Rao, G.M. Reddy, Control of Laves phase in Inconel 718 GTA welds with current pulsing Control of Laves phase in Inconel 718 GTA welds with current pulsing, Sci. Technol. Weld. Join. 9 (2004) 390–398. https://doi.org/10.1179/136217104225021788.

[16] J.J. Schirra, R.H. Caless, R.W. Hatala, THE EFFECT OF LAVES PHASE ON THE MECHANICAL, in: Superalloys 718, 625 Var. Deriv., 1991: pp. 375–388.

[17] S. Sui, J. Chen, E. Fan, H. Yang, X. Lin, W. Huang, The influence of Laves phases on the high-cycle fatigue behavior of laser additive manufactured Inconel 718, Mater. Sci. Eng. A. 695 (2017) 6–13. https://doi.org/10.1016/j.msea.2017.03.098.

[18] D. Kong, C. Dong, X. Ni, L. Zhang, C. Man, J. Yao, Y. Ji, Y. Ying, K. Xiao, X. Cheng, X. Li, High-throughput fabrication of nickel-based alloys with different Nb contents via a dual-feed additive manufacturing system: Effect of Nb content on microstructural and mechanical properties, J. Alloys Compd. 785 (2019) 826–837. https://doi.org/10.1016/j.jallcom.2019.01.263.

[19] H. Xiao, S.M. Li, W.J. Xiao, Y.Q. Li, L.M. Cha, J. Mazumder, L.J. Song, Effects of laser modes on Nb segregation and Laves phase formation during laser additive manufacturing of nickel-based superalloy, Mater. Lett. 188 (2017) 260–262. https://doi.org/10.1016/j.matlet.2016.10.118.

[20] T.G. Gallmeyer, S. Moorthy, B.B. Kappes, M.J. Mills, B. Amin-Ahmadi, A.P. Stebner, Knowledge of process-structure-property relationships to engineer better heat treatments for laser powder bed fusion additive manufactured Inconel 718, Addit. Manuf. 31 (2020) 1–18. https://doi.org/10.1016/j.addma.2019.100977.

[21] S. Sridar, Y. Zhao, W. Xiong, Phase Transformations During Homogenization of Inconel 718 Alloy Fabricated by Suction Casting and Laser Powder Bed Fusion: A CALPHAD Case Study Evaluating Different Homogenization Models, J. Phase Equilibria Diffus. 42 (2021) 28–41. https://doi.org/10.1007/s11669-021-00871-3.

[22] S. Sui, J. Chen, Z. Li, H. Li, X. Zhao, H. Tan, Investigation of dissolution behavior of laves phase in inconel 718 fabricated by laser directed energy deposition, Addit. Manuf. 32 (2020) 101055. https://doi.org/10.1016/j.addma.2020.101055.

[23] W.M. Tucho, P. Cuvillier, A. Sjolyst-kverneland, V. Hansen, Materials Science & Engineering A Microstructure and hardness studies of Inconel 718 manufactured by selective laser melting before and after solution heat treatment, Mater. Sci. Eng. A. 689 (2017) 220–232. https://doi.org/10.1016/j.msea.2017.02.062.

[24] D. Zhang, W. Niu, X. Cao, Z. Liu, Materials Science & Engineering A Effect of standard heat treatment on the microstructure and mechanical properties of selective laser melting manufactured Inconel, Mater. Sci. Eng. A. 644 (2015) 32–40. https://doi.org/10.1016/j.msea.2015.06.021.

[25] R.R. Dehoff, M.M. Kirka, W.J. Sames, H. Bilheux, A.S. Tremsin, L.E. Lowe, S.S. Babu, M.M. Kirka, W.J. Sames, H. Bilheux, A.S. Tremsin, R.R. Dehoff, M.M. Kirka, W.J. Sames, H. Bilheux, A.S. Tremsin, Site specific control of crystallographic grain orientation through electron beam additive manufacturing Site specific control of crystallographic grain orientation through electron beam additive manufacturing, Mater. Sci. Technol. (United Kingdom). 0836 (2015). https://doi.org/10.1179/1743284714Y.0000000734.